Sahlgrenska Academy

Optimization of Kidney Dosimetry: Determination of Recovery Coefficient for Kidneys and SPECT/CT Imaging of [^{177}Lu]Lu-DOTATATE/TOC

Master's thesis in Medical Physics

Vanessa Becker
Department of Medical Radiation Sciences
University of Gothenburg
Gothenburg, Sweden 2025

Master's Thesis 2025

Optimization of Kidney Dosimetry: Determination of Recovery Coefficient for Kidneys and SPECT/CT Imaging of [^{177}Lu]Lu-DOTATATE/TOC

Vanessa Becker

UNIVERSITY OF
GOTHENBURG

Sahlgrenska academy
Institute of Clinical Sciences
Department of Medical radiation sciences
University of Gothenburg
Gothenburg, Sweden 2025

Optimization of Kidney Dosimetry: Determination of Recovery Coefficient for Kidneys and SPECT/CT Imaging of [^{177}Lu]Lu-DOTATATE/TOC
Vanessa Becker

Supervisor: Linn Hagmarker, PhD[1], Johanna Dalmo, PhD[1]
Examiner: Magnus Båth, Professor[2]

Affiliations: [1]Department of Biomedical Engineering and Medical Physics, Sahlgrenska University Hospital, Gothenburg, Sweden
[2]Department of Medical Radiation Sciences, Institute of Clinical Sciences, Sahlgrenska Academy, University of Gothenburg, Gothenburg, Sweden.

Master's Thesis 2025
Institute of Clinical Sciences
Department of Medical Radiation Sciences
University of Gothenburg
Gula stråket 2B SU/Sahlgrenska
SE-41345 Gothenburg

Typeset in LaTeX
Gothenburg, Sweden 2025

Optimization of Kidney Dosimetry: Determination of Recovery Coefficient for Kidneys and SPECT/CT Imaging of [^{177}Lu]Lu-DOTATATE/TOC

Vanessa Becker
Department of Medical radiation sciences
University of Gothenburg

Abstract

Purpose: Peptide receptor radionuclide therapy (PRRT) with [^{177}Lu]Lu-DOTATATE/TOC is an effective treatment for neuroendocrine tumors, but this treatment also involves an unwanted radiation dose to the kidneys. Dosimetry can be used to optimize treatment and reduce kidney toxicity, and therefore, obtaining an accurate estimate of activity concentration in the kidneys is essential. One of the main challenges in quantitative SPECT imaging for dosimetry is the partial volume effect, which leads to an underestimation of activity. This effect can be corrected for by using a recovery coefficient (RC). The study aimed to obtain an RC for kidneys using a software developed by Hermes for organ and tumor dosimetry. The study investigates how the RC is affected by different activity concentrations in the kidneys and the ratio between the activity concentration in the kidney and the background. It was also studied how the RC is affected by different reconstruction methods and two different projection sets, 30 and 60 projections.

Method: Five 3D-printed kidney phantoms were filled with [^{177}Lu]Lu-DOTATATE/TOC and placed in either a Jaszczak phantom or a NEMA phantom. Different activity concentrations were investigated as well as different ratios between the activity concentration in the kidney and the background. Images were collected with a SPECT/CT system (GE Healthcare Discovery NM/CT 670 Pro) and reconstructed in Hermes (Hermia Hybrid Recon 5.0.) using Ordered Subset Expectation Maximization (OSEM) and Relative Difference Prior (RDP). The kidneys were manually segmented, and the RC was determined for each measurement. In addition, the RC was compared between different segmentation methods i.e. the whole kidney segmented volume of interest (VOI), and the small VOI method was examined.

Results: The RC was not statistically significantly affected by variations in activity concentration or kidney-to-background ratios. However, a statistically significant difference was shown between the two reconstruction methods, where reconstruction using RDP resulted in a higher RC than when reconstructing images with OSEM. A statistically significant difference was also found between 30 and 60 projections, probably due to increased noise in 30 projections. When comparing various activity concentrations, the whole kidney segmentation approach's standard deviation was smaller than that of the small VOIs method. At Sahlgrenska University Hospital, the RC was determined to be 0.80 with whole kidney segmentation, 60 projections collected and reconstructed with RDP.

Conclusion: The RC for kidneys in SPECT/CT imaging with [^{177}Lu]Lu-DOTATATE/TOC are stable across the investigated range of activity concentrations and background ratios, supporting the use of a standardized RC for all imaging time points for whole kidney segmentation in dosimetry. At Sahlgrenska University Hospital, the RC was determined to be 0.80 and the method for determination of the RC is considered reasonable.

Sammanfattning

Syftet: Peptidreceptor-radionuklidterapi (PRRT) med [^{177}Lu]Lu-DOTATATE/TOC är en effektiv behandling för neuroendokrina tumörer, men denna behandling medför också en oönskad stråldos till njurarna. Dosimetri kan användas för att optimera behandlingen och minska njurtoxiciteten, och därför är det avgörande att få en noggrann uppskattning av aktivitetskoncentrationen i njurarna. En av de största utmaningarna inom kvantitativ SPECT för dosimetri är den så kallade partiella volymseffekten, som leder till en underskattning av aktiviteten. Denna effekt kan korrigeras med hjälp av en recovery-koefficient (RC). Syftet med studien var att ta fram en RC för njurar med hjälp av en programvara utvecklad av Hermes för dosimetri av organ och tumörer. Studien undersökte hur RC påverkas av olika aktivitetskoncentrationer i njurarna samt förhållandet mellan aktivitetskoncentrationen i njurarna och i bakgrunden. Det studerades även hur RC påverkas av olika rekonstruktionsmetoder och två olika uppsättningar av projektioner, 30 respektive 60 projektioner.

Metod: Fem 3D-printade njurfantom fylldes med [^{177}Lu]Lu-DOTATATE/TOC och placerades antingen i ett Jaszczak-fantom eller ett NEMA-fantom. Olika aktivitetskoncentrationer samt olika förhållanden mellan aktivitetskoncentrationen i njurarna och i bakgrunden undersöktes. Bilder samlades in med ett SPECT/CT-system (GE Healthcare Discovery NM/CT 670 Pro) och rekonstruerades i Hermes (Hermia Hybrid Recon 5.0) med hjälp av Ordered Subset Expectation Maximization (OSEM) och Relative Difference Prior (RDP). Njurarna segmenterades manuellt och RC bestämdes för varje mätning. Dessutom jämfördes RC mellan olika segmenteringsmetoder, dels hela njurens segmenterade volym (VOI), dels den så kallade small VOI-metoden.

Resultat: RC påverkades inte statistisk signifikant av variationer i aktivitetskoncentration eller förhållandet mellan njure och bakgrund. Däremot påvisades en statistisk signifikant skillnad mellan de två rekonstruktionsmetoderna, där rekonstruktion med RDP resulterade i en högre RC jämfört med rekonstruktion med OSEM. En statistisk signifikant skillnad observerades även mellan 30 och 60 projektioner, troligen på grund av ökad brusnivå vid 30 projektioner. Vid jämförelse av olika aktivitetskoncentrationer var standardavvikelsen för hela njurens segmentering mindre än för small VOI-metoden. På Sahlgrenska Universitetssjukhuset fastställdes RC till 0,80 med helnjursegmentering, 60 projektioner insamlade och rekonstruerade med RDP.

Slutsats: RC för njurar vid SPECT/CT-avbildning med [^{177}Lu]Lu-DOTATATE/TOC är stabil inom det undersökta intervallet av aktivitetskoncentrationer och bakgrundsförhållanden, vilket stödjer användningen av en standardiserad RC för samtliga avbildningstillfällen vid helnjuresegmentering i dosimetri. Vid Sahlgrenska Universitetssjukhuset fastställdes RC till 0,80 och metoden för bestämning av RC anses rimlig.

Keywords: Kidney dosimetry, Segmentation, Recovery coefficient, [^{177}Lu]Lu-DOTATATE, Nuclear Medicin, Activity concentration, OSEM, RDP, Hermes

Acknowledgements

I want to thank my main supervisor, Linn Hagmarker, and my co-supervisor, Johanna Dalmo, for all their help and guidance during this project. I would also like to thank them for always being able to discuss any questions, no matter how unusual the questions were.

I would also like to thank the employees at 3D Teknik Medicinsk Teknik Mölndal and Radiologisk Teknik at Sahlgrenska, especially Johan Andersson, for all the kidneys that were printed for this work. I would also like to thank Lovisa Jessen for the kidney manual for the 3D printing.

Last but not least, I would like to thank my fantastic partner, Joel Hildingsson, who has supported me throughout my education and has heard me talk about this work a thousand times. Thank you for always believing in me when I doubted myself.

List of Acronyms

Below is the list of acronyms that have been used throughout this thesis listed in alphabetical order:

CF	Calibration factor
CT	Computed tomography scan
MLEM	Maximum likelihood expectation maximization
NETs	Neuroendocrine tumors
OSEM	Ordered subset expectation maximization
PVE	Partial volume effect
PRRT	Peptide receptor radionuclide therapy
RC	Recovery coefficient
RDP	Relative difference prior
SNR	Signal-to-noise ratio
SPECT	Single-photon emission computed tomography
SSTR	Somatostatin receptor
VOI	Volume of interest
[^{177}Lu]-DOTATATE	[^{177}Lu]Lu-DOTATATE/TOC

Contents

1 Background and Theory

1.1 NETs and [^{177}Lu]Lu-DOTATATE/TOC treatment

Neuroendocrine tumors (NETs) develop from neuroendocrine cells and are most commonly found in the gastrointestinal tract, lungs, and pancreas [1]. Even if NETs are declared rare, they have become more common, with an increased incidence per 100,000 people from 4.9 in 2000 to 8.19 in 2018, mainly due to improved detection [2][3][4]. An effective treatment is peptide receptor radionuclide therapy (PRRT) that targets the somatostatin receptor (SSTR) in tumors and in organs within the neuroendocrine system [5]. The [^{177}Lu]Lu-DOTATATE/TOC ([^{177}Lu]-DOTATATE) consists of a somatostatin analog (a protein) which is combined via a chelating molecule to the radionuclide, and the molecule binds to tumor cells via SSTR [6]. When the peptide is attached to tumor cells, the radiopharmaceuticals are internalized into the tumor cell and damage its DNA through radiation-induced single and double-stranded DNA breaks, which eventually leads to apoptosis of the cancer cell, as seen in Figure 1 [7][8].

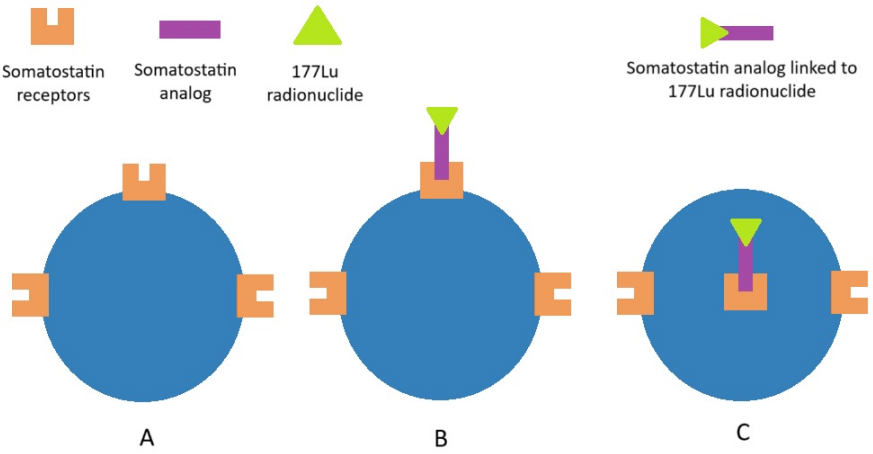

Figure 1: *Simplified overview of the PRRT using ^{177}Lu as the radionuclide. A: the cancer cells with somatostatin receptors on the surface. B: ^{177}Lu linked to a peptide with a somatostatin analog, attaching to the cancer cells' somatostatin receptors. C: Through the peptide, ^{177}Lu embodies the cell and emits β-radiation, which destroys the cancer cell from the inside.*

There are currently two radionuclides that are used in PRRT, Yttrium-90 (^{90}Y) and Lutetium-177 (^{177}Lu), which are combined with tetracarboxylic acid (DOTA). It has been shown that due to its more extended β-particle range, ^{90}Y is more suitable for treating larger tumors while ^{177}Lu is more ideal for smaller tumors [9]. ^{177}Lu is more widely used since it emits lower energy and has better dose uniformity for smaller tumors, which endocrine tumors often are [10]. It has also been shown that due to ^{90}Y long-range β-particles, toxicity is lower for ^{177}Lu. ^{90}Y has a higher absorbed dose to both the kidneys and bone marrow [11]. ^{177}Lu has a half-life of 6.4 days and a maximal penetration of 2 mm in normal tissue. It does not only emit β-radiation ($E_{\beta_{max}}$ of 498.3 keV) but also low-energy γ-radiation (E_γ of 208 keV and 113 keV), which is used in Single-photon emission computed tomography (SPECT)

and image-based dosimetry [6].

[^{177}Lu]-DOTATATE-treament is generally divided into four treatment cycles, one cycle every eight to twelve weeks, and is given as an intravenous infusion together with kidney protective amino acids. The administered activity is 7.4 GBq (± 10 %) per cycle. The treatment is shown to be effective against NETs with minor side effects. The kidneys and bone marrow are organs at risk, and adjustments in administered activity, time between cycles, and number of cycles can be necessary depending on the patient's hematologic response, which depends on the irradiation on the bone marrow and the kidneys [7][12].

Several dosimetry-guided studies have shown that additional cycles can be given without damaging the kidneys [13][14]. So, dosimetry can be a guide to optimize PRRT. If the doses to tumors and normal tissues are known, the risk of under-treatment and toxicity, respectively are lower. There is an ongoing study called START-NET, which is a collaboration between Lund, Uppsala, Stockholm, and Gothenburg, aiming to compare the standard protocol of 4 treatment cycles and a patient-specific protocol based on kidney dosimetry. The treatment will proceed until the kidney dose limit (27 Gy) is reached up to 9 treatment cycles.

1.2 Anatomy of the kidney

The kidneys are located in the retroperitoneal space and are part of the urinary system [15]. The kidney's main function is to control the volume of various body fluids by filtration and eventually eliminate excess body fluid. Ammonium, potassium, hydrogen, and uric acid are some of the most common substances secreted. Substances not removed from the body are reabsorbed, such as proteins for example somatostatin and its analogs, sodium, glucose, amino acids, bicarbonate, and solute-free water.

The kidneys are divided into two major structures, the renal cortex and the renal medulla [16]. A simplified kidney structure can be seen in Figure 2A. The cortex is the outer region of the kidney and surrounds the renal medulla, which is the inner region of the kidney [17]. The renal medulla is split into pyramid-shaped structures called renal pyramids [18]. The basic structural and functional component of the kidney that filters waste from the blood and creates urine is called a nephron [19]. The nephron starts in the renal cortex and continuous in the renal medulla [18]. A simplified nephron structure can be seen in Figure 2B.

The cortex contains glomeruli and proximal and distal tubules [20]. The glomerulus is the primary filtration in the kidney, which is formed by small capillaries. Surrounding the glomerulus is Bowman's capsule, which is located at the beginning of a nephron. Glomerulus and Bowman's capsules are essential for blood filtering [21]. Immediately after the Bowman's Capsule is the proximal tubule, which is responsible for reabsorbing organic nutrients such as water, glucose, and amino acids. Organic anions such as hydrogen and ammonium are also secreted [22]. Reabsorption and se-

cretion occur in the distal tubule, but to a lesser extent than in the proximal tubule. Here, sodium, calcium and chloride are reabsorbed, while potassium is secreted [23].

The renal medulla contains Henle's loop, collecting ducts, and Vasa recta. Henle's loop helps absorb water in collecting ducts by creating salt through a countercurrent multiplier process. With the help of the antidiuretic hormone (ADH), water is reabsorbed in collecting ducts to prevent dehydration. Vasa recta maintain the osmotic gradient, which is required for water absorption [17]. The nephron is the key to making filtration possible and is the structure that removes the waste substances from blood and produces urine [19]. The collecting duct is the final segment that transports urine into the renal pelvis and ureters after collecting it from the nephrons [24]. Other significant roles for the kidney are to produce the hormones erythropoietin and renin, which stimulate the production of the red blood cells in the bone marrow respective to an enzyme that helps to control the body's blood pressure and maintain a normal level of potassium and sodium in the body [25][26].

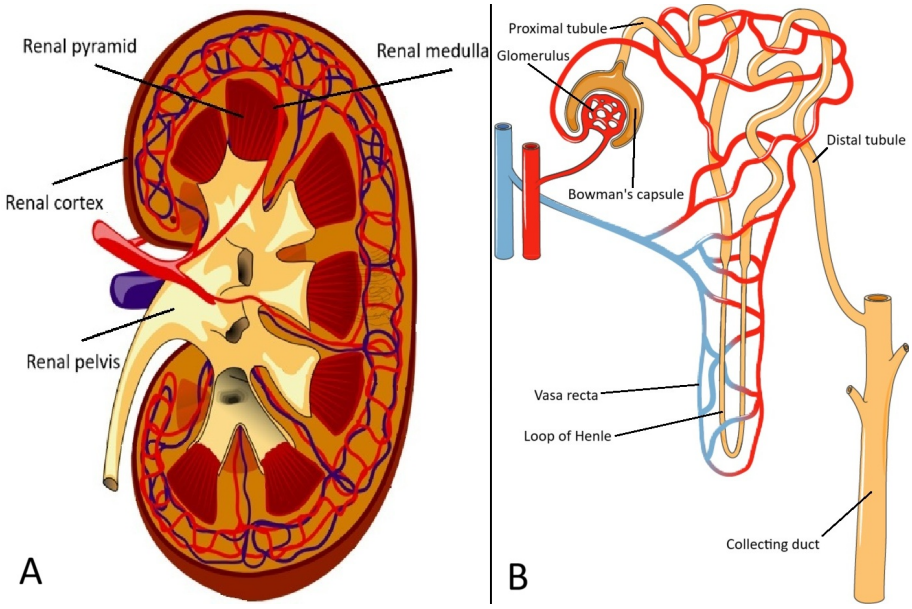

Figure 2: *A: Simplified structure of the kidney where it is shown that the medulla consists of pyramids and is surrounded by the cortex. After filtration, the urine flows from the renal pelvis to the ureter. Modified from Kidney by PioM, licensed under CC BY-SA 3.0 via Wikimedia Commons.[27]*
B: A nephron showing that Bowman's capsule surrounds the glomerulus. The proximal tubule starts from Bowman's capsule, which becomes Henle's loop, and then the distal tubule. Finally, everything ends up in the collecting duct. Modified from Urinary system – Nephron 2 by Smart Servier Medical Art, licensed under CC BY 3.0 via Wikimedia Commons.[28]

1.3 Kidney dosimetry

In treatment, [^{177}Lu]-DOTATATE is reabsorbed into the bloodstream via the proximal tubule which results in an accumulated dose to the kidneys. To reduce the reabsorption, an amino acid is given to the patient during the [^{177}Lu]-DOTATATE infusion. Despite the use of amino acids, the kidneys can receive high absorbed doses.

The absorbed dose to the kidneys varies between individuals due to differences in kidney function, pharmacokinetics, and tumor burden; individualized kidney dosimetry is essential to optimize therapeutic efficacy while minimizing nephrotoxicity [29].

The first step in the clinical dosimetry workflow (Figure 3) is calibration acquisitions. The dose calibrator and the gamma camera must be properly calibrated. Calibration acquisitions implies calibration measurements to obtain the calibration factor (CF). Patient data is collected with chosen acquisition parameters and reconstruction methods. According to EANM, 60-120 projections are recommended, but the number of projections may be decreased to estimate the activity concentration in centrally placed, high-uptake tissues [30]. A higher number of projections and longer frame duration takes longer but provides better statistics and, thus, a better image [31]. The two reconstruction methods used in this study are presented in section 1.4.1 and 1.4.2.

SPECT is often combined with a computed tomography scanner (CT) to obtain an image of the anatomical structure, which is also used for attenuation correction [32]. CF is then used to convert counts per second in the image into activity units. The CF is based on measured counts during a certain time in the camera and known activity in a homogeneous cylindrical phantom [33].

Imaging at several time points enables the assessment of activity clearance in regions or volumes of interest (VOIs) [34]. Segmentation can be performed by segmenting the entire kidney (whole organ segmentation) or small VOI segmentation. Small VOI segmentation means placing small VOIs in the kidney and using the average VOIs average activity concentration when calculating activity [35]. The advantage of this method is that it is time-efficient compared to manual segmentation of the entire kidney, though AI algorithms for whole organ segmentation are now available. Time-activity curves are created from activity concentrations in SPECT images. These can then be used to calculate the absorbed dose using established dosimetry models [29][36]. In addition to the direct energy deposition, there are two other commonly used methods for determining the absorbed dose: one is to use computational algorithms such as Monte Carlo simulations to model radiation transport and energy deposition in tissues; the other is to apply pre-calculated dose conversion factors, such as the S-values used in the MIRD formalism [34].

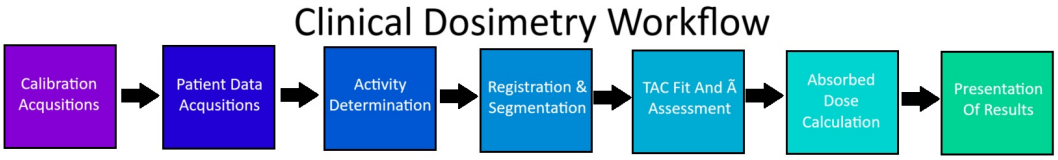

Figure 3: *The clinical dosimetry workflow. This study delves into Activity Determination and Registration & Segmentation*

One of the key challenges with kidney dosimetry is that the measured activity concentration in the kidney may be underestimated due to partial volume effects (PVE). Partial volume effect is a measurement error of activity concentration on objects two times smaller than the full width at half maximum (FWHM) of a gamma camera [37]. In such cases, the system cannot fully distinguish the activity within the object from its surroundings. This leads to inaccurate quantification, where the measured activity appears over or underestimated. This can be adjusted for with a recovery coefficient (RC). Spill-out occurs because photons emitted from a small object are registered in adjacent voxels. This contributes to the fact that it appears that the activity has spilled out of the object, resulting in an underestimation of activity in the object and an overestimation in the background. A smaller object thus increases the likelihood of the spill-out effect and, therefore, the RC will decrease. However, a spill-in impact may occur if there is a background with high activity. In that case, photons from the surrounding environment spill into the object's measured volume and thus increase the measured activity in the object. This can lead to an increased RC [33][38][39]. In addition to the spatial resolution, PVE also depends on image acquisition and tumor/organ shape and volume [39][40].

The RC is a quantitative correction factor to account for the PVE and is defined as the ratio between the measured activity concentration and the true activity concentration within a VOI, according to Equation 1

$$RC = \frac{AC_{Measured}}{AC_{True}} \tag{1}$$

where $AC_{Measured}$ is the measured activity concentration using SPECT/CT and AC_{True} is the known activity [40]. In ideal conditions, this ratio should be 1.0, meaning that the measured activity concentration is the same as the true concentration. However, this is rarely the case due to limitations in imaging system resolution, especially for small structures [39].

To improve kidney dosimetry, 3D-printed kidneys are often used in studies today. It is shown that 3D-printed kidney phantoms are promising for geometry-specific calibration of SPECT/CT systems [41]. The advantage of a 3D-printed kidney is that the material cost is low compared to traditional phantoms such as NEMA and Jaszack. In addition, there is a greater opportunity for individual customization with 3D-printed phantoms [42].

1.4 Hermes Medical Solution-Voxel dosimetry

The dosimetry workflow in voxel dosimetry in Hermia includes alignment of multiple SPECT/CT, calculation of the accumulated activity in each voxel at voxel or organ level, an artificial intelligence (AI) based organ segmentation, and calculation of absorbed dose [43]. To be able to use segmentation of the whole kidneys in Hermes, the RC must be determined to compensate for the PVE. Hermes Medical Solution has developed a nuclear medicine molecular imaging software named Hermia that includes reviewing, reconstruction, and processing [44]. Hermia Recon is a recon-

struction tool that contains Monte Carlo-based attenuation, scatter correction and collimator response [45].

1.4.1 Ordered Subset Expectation Maximization

Ordered Subset Expectation Maximization (OSEM) is the most common iterative reconstruction method used in nuclear medicine images. OSEM uses the Maximum Likelihood Expectation Maximization (MLEM) algorithm with an ordered subset acceleration and is defined as

$$f_j^{new} = \frac{f_j^{old}}{\sum_{i \epsilon S_n} a_{ij}} \sum_{i \epsilon S_n} a_{ij} \frac{p_i}{\sum_k a_{ik} f_k^{old}} \tag{2}$$

where f_{new} is the image estimate, f_{old} is the old image estimate, i is the projection pixel index, j and k are the reconstruction voxel index, p is the projections and a_{ij} is the probability that a photon emitted from voxel j or k is detected in projection pixel i. Equation 2 is built up of a penalty factor, which introduces regularization (Equation 3) and an OSEM update factor (Equation 4) [46].

$$\frac{1}{\sum_{i \epsilon S_n} a_{ij}} \tag{3}$$

$$\sum_{i \epsilon S_n} a_{ij} \frac{p_i}{\sum_k a_{ik} f_k^{old}} \tag{4}$$

OSEM can include modeling of the physical properties of the image processing, such as compensation for photon scattering, photon attenuation, and detector response. An important factor within OSEM is the number of updates defined according to

$$N_{update} = N_{subsets} \cdot N_{iterations} \tag{5}$$

where $N_{subsets}$ is the number of subsets and $N_{iterations}$ is the number of iterations. Increasing the total number of updates (defined as the product of iterations and subsets) improves the accuracy of the quantitative activity recovery as the reconstruction progresses toward convergence. However, this also increases image noise since standard OSEM does not include noise suppression mechanisms. For this reason, OSEM is often terminated after a limited number of updates to avoid excessive noise, even if this results in incomplete recovery of activity values, especially in small structures [33].

1.4.2 Relative difference prior

Relative Difference Prior (RDP) is a regularization method, typically used in Penalized OSEM, that preserves edges while reducing image noise using Bayesian reconstruction algorithms, also known as Maximum a posteriori. The method uses the introduction of constraints, which are prior information about what the reconstructed image is expected to look like. This is introduced into the reconstruction problem, meaning the solution is guided in a certain direction. Maximum a posteriori is then combined with iterative reconstruction through the One Step Late algorithm described as follows

$$f_j^{new} = \frac{f_j^{old}}{\sum_{i \epsilon S_n} a_{ij} + \beta \frac{\partial U(f^{old})}{\partial (f^{old})}} \sum_{i \epsilon S_n} a_{ij} \frac{p_i}{\sum_k a_{ik} f_k^{old}} \tag{6}$$

The equation is similar to the equation for OSEM, but includes the previous weighting term β multiplied by the derivative of the energy function U in the penalty factor. The penalty factor for RDP is defined according to the following Equation

$$c_j^p = \frac{1}{\sum_{i \epsilon S_n} a_{ij} + \beta \sum_{k \epsilon N_j} \frac{(f_j - f_k)(\gamma |f_j - f_k| + f_j + 3f_k)}{(f_j + f_k + \gamma |f_j + f_k|)^2}} \tag{7}$$

where the γ controls the degree of edge preservation [46]. While OSEM follows Hermes recommendations, the RDP settings are from Lund, where they have been using Hermes for a while now.

1.5 Aim

The aim of the study was to determine the RC for kidney dosimetry in Hermes by using 3D-printed nonuniform anthropomorphic kidney phantoms. The aim was also to determine if the RC was dependent on the kidney's activity concentration to answer whether the RC can be used for all imaging time points. It was also studied if the RC is affected by the ratio between the activity concentration in the kidney and the background. In addition, the RC was evaluated using two different reconstruction methods and two data sets: one dataset with 30 projections and one with 60 projections.

2 Materials and Method

2.1 Image Acquisition

The gamma camera was a GE Healthcare Discovery NM/CT 670 Pro with a medium energy general purpose collimator. SPECT imaging was performed using a 40-second frame duration for two separate collections, 30 and 60 projections, and the energy windows were set to 113 kV ±10% and 208 kV ±10%.

Both 30 and 60 projections were reconstructed with Ordered Subset Expectation Maximization (OSEM) and Relative Difference Prior (RDP) in Hermia Hybrid Recon 5.0. 30 projections used 14 iterations and 6 subsets, while 60 projections had 8 iterations and 10 subsets. The CF was determined using a cylinder phantom filled with [^{177}Lu]-DOTATATE [47]. 30 projections had a CF of 13.8 while 60 projections had a CF of 14.0. All settings are found in Appendix Table 4.

2.2 Kidney phantom

Four acrylic kidneys were 3D printed at 3D Teknik Medicinsk Teknik Mölndal and Radiologisk Teknik at Sahlgrenska and one in Lund. All five kidneys were printed using the same kidney template. The kidneys from Mölndal were made from Dental LT clear V1, and the kidney from Lund was made from clear V4 resin. Three were made to fit a Data Spectrum ECT phantom (Jaszczak phantom) and two for a NEMA IEC PET Bodyphantom (NEMA phantom). Each kidney consisted of the cortex, medulla, and renal pelvis. The cortex was hollow, and the medulla was made using a grid-based technique to obtain a non-homogeneous activity distribution. The kidney phantoms can be seen in Figure 4. One kidney was printed to study how the RC varies with activity concentration. Two kidneys were printed to study how the RC varies with the ratio where a higher activity concentration was used. The remaining two kidneys were also used to investigate how the RC varies with the ratio where however the activity concentration was lower.

The fillable volume for each kidney was determined by weighing the kidneys before and after filling them with water. Since the medulla, which is not fillable, takes up a large portion of the total volume during segmentation, its volume also needed to be determined. All kidneys were additionally printed without the medulla to estimate the volume of the medulla. The difference in weight between the kidney with medulla and the kidney without medulla gave the medulla weight. The weight was then divided by the density of the material, which was 1.10 g/mL – 1.20 g/mL, to obtain the volume of each medulla. This was performed for each kidney. The medullary volume was added to the fillable volume to obtain the total volume of the kidney. The weights and the volumes for each kidney can be seen in Table 1. With the kidneys placed in the phantom, the fillable volume of the Jaszczak phantom was 6.47 L, and 9.89 L for the NEMA phantom. Ethylenediaminetetraacetic acid (EDTA) was added to the water solution in the Jaszczak, NEMA and the kidney phantoms, to prevent [^{177}Lu]-DOTATATE from sticking to the plastic on the phantoms.

Figure 4: *Kidney 4 (left) and kidney 5 (right).*

Table 1: The weights and volumes of each kidney.

	Empty weight with medulla [g]	Medulla weight [g]	Fillable volume [mL]	Total volume [mL]
Kidney 1	56.93	25.03	84.00	106.00
Kidney 2	87.94	45.48	75.00	114.67
Kidney 3	78.71	39.98	75.00	109.87
Kidney 4	89.60	40.81	75.00	110.59
Kidney 5	84.10	38.53	80.00	113.61

2.3 Segmentation and RC calculation

Kidney 1, the kidney from Lund, was filled with an activity of 83.05 MBq, which gave an activity concentration of 0.78 MBq/mL. The kidney was placed in a Jaszczak phantom. The activity concentration was chosen based on patient data. The first SPECT/CT was collected without background activity. The Jaszczak phantom was then filled with an activity of 354 MBq, which gave a background activity concentration of 0.06 MBq/mL and a ratio of 13.61 between the activity concentration in the kidney and the background. The set-up of the kidney in the Jaszczak phantom is shown in Figure 5. Seven measurements were made during 3 weeks until the activity concentration was comparable to the activity concentration in the kidneys in patients on day 7. SPECT reconstruction was performed as described in section 2.1

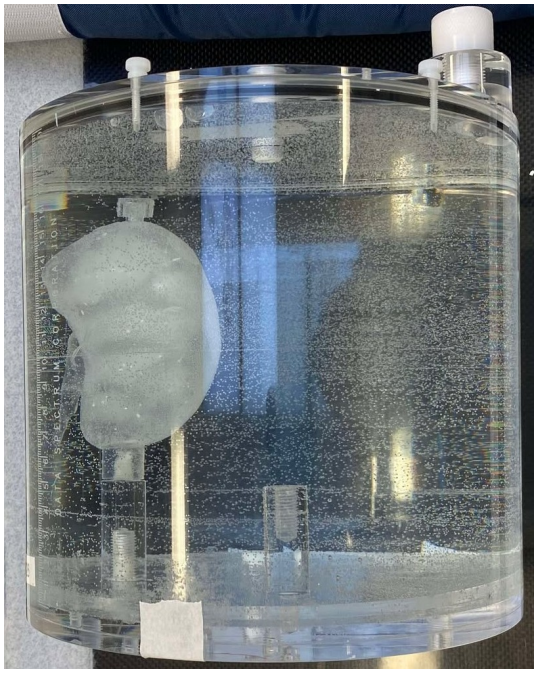

Figure 5: *Kidney 1 placed in the Jaszczak phantom.*

The AI-based segmentation tool in Hermes voxel dosimetry could not be used for phantoms, and kidney VOIs were, therefore, manually segmented in Affinity in Hermes. Segmentation of one of the kidneys can be seen in Figure 6. The RC was calculated using Equation 1. A comparison between the two reconstruction methods and the two datasets with 30 and 60 projections was performed using a Student's t-test.

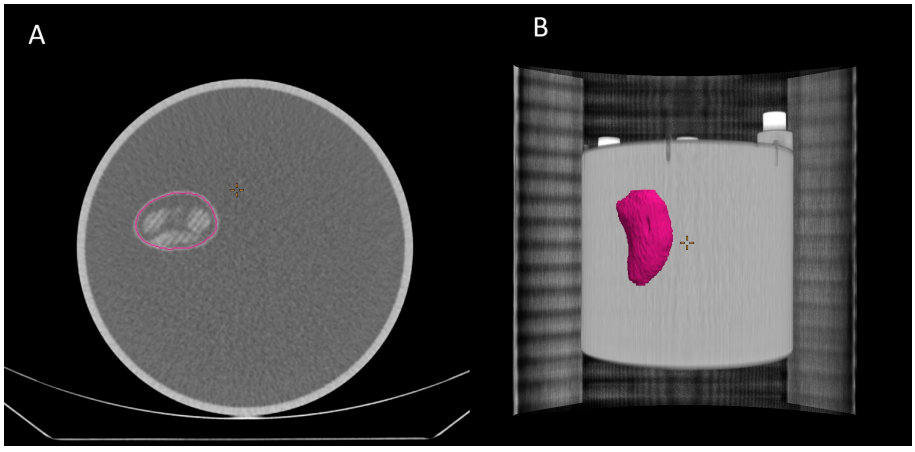

Figure 6: *A: Segmentation of kidney 1 in the Jaszczak phantom in the CT image. B: 3D image of the segmentation of the kidney.*

SPECT images were collected with different ratios between the activity concentration in the kidneys and the background to see how the background activity concentration affects the RC. On day 0, kidneys 2, 3, 4, and 5 were filled with [^{177}Lu]-DOTATATE; the activities can be seen in Table 2. Kidneys 2 and 3 were placed in a Jaszczak phantom, while kidneys 4 and 5 were placed in a NEMA phantom.

Images were collected on days 1, 2, 3 and 4. On day 1, there was no background activity. On day 2, [^{177}Lu]-DOTATATE was added to the background, aiming for a ratio of 25. On days 3 and 4, additional [^{177}Lu]-DOTATATE was added, aiming for ratios at 15 and 5. The ratio varied from kidney to kidney since each kidney has individual volumes. The ratios are shown in Table 3. The Jaszczak and NEMA phantoms were always filled with [^{177}Lu]-DOTATATE the day before, allowing 20-24 hours to achieve a homogeneous activity distribution. The set-up of the kidneys, both for the Jaszczak and the NEMA phantom, is shown in Figure 7. Imaging and reconstruction were performed as described in section 2.1.

Table 2: The total activity and the activity concentration for the entire kidney are displayed for each kidney.

	Total activity $[MBq]$	Total AC $[MBq/mL]$
Kidney 1	83.05	0.78
Kidney 2	81.86	0.71
Kidney 3	81.84	0.75
Kidney 4	40.88	0.37
Kidney 5	44.06	0.39

Table 3: The ratio between the whole kidney and the background.

Ratio	Low background	Medium background	High background
Kidney 2	16.44	9.46	3.17
Kidney 3	17.15	9.87	3.31
Kidney 4	16.48	9.69	3.29
Kidney 5	17.29	10.17	3.46
Mean ratio	16.84	9.80	3.31

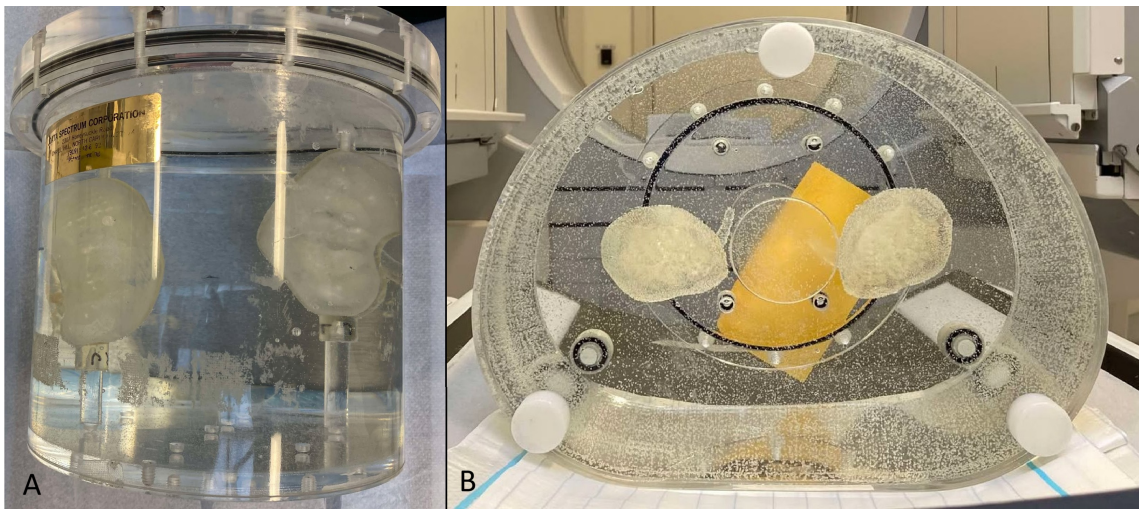

Figure 7: *A: Kidney 2 and 3 in the Jaszczak phantom from the front. B: Kidney 4 and 5 in the NEMA phantom from below.*

The segmentation of kidneys 2 and 3 in the Jaszczak phantom can be seen in Figure 8 and the segmentation of kidneys 4 and 5 in the NEMA phantom in Figure 9. The

mean activity concentration was extracted for each kidney in Hermia Affinity 4.0.1. The RC for each measurement was derived from Equation 1.

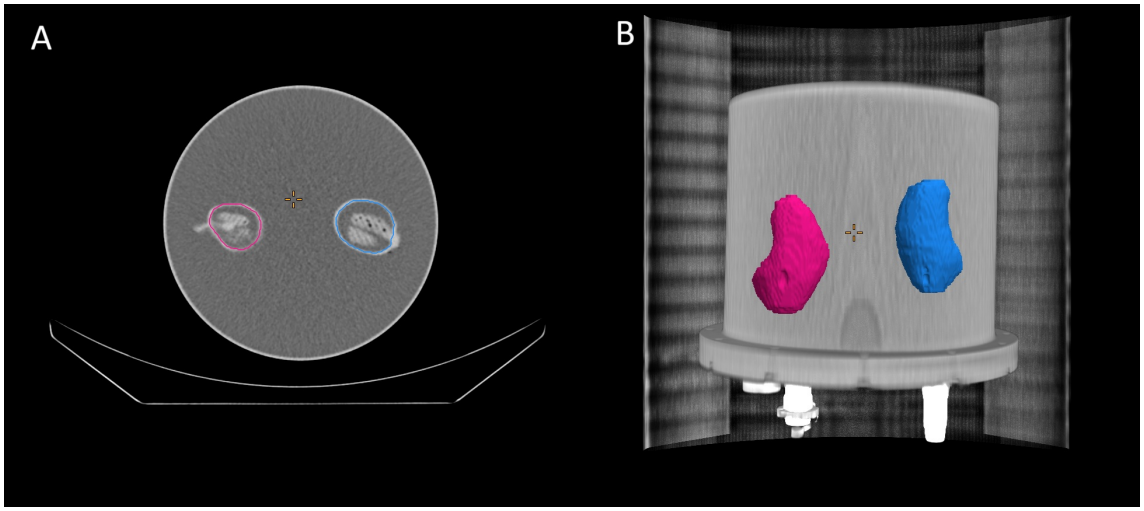

Figure 8: *A: Segmentation of kidney 2 and 3 in the Jaszczak phantom in the CT image. B: 3D image of the segmentation of the kidneys.*

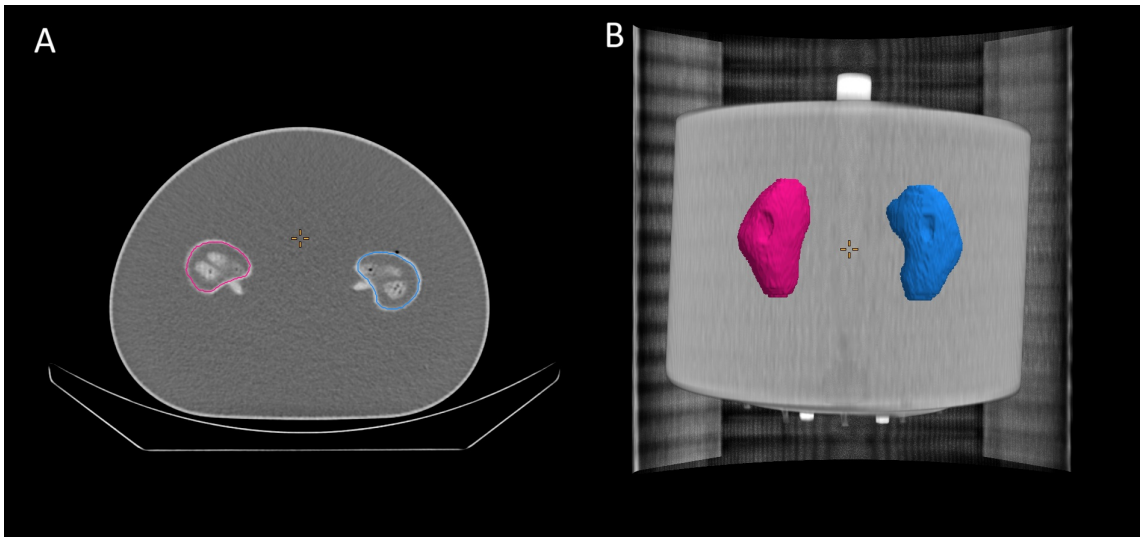

Figure 9: *A: Segmentation of kidney 4 and 5 in the NEMA phantom in the CT image. B: 3D image of the segmentation of the kidneys.*

2.4 Recovery using small VOI method

The small VOI method was performed to compare with the whole kidney segmented method, this was investigated for kidney 1 in section 2.3. Five VOIs of 2 mL were placed in the kidney in different slices. The mean activity concentration from the five VOIs was used to estimate the RC.

3 Results

The RC did not vary with the activity concentration in kidney 1, as seen in Figure 10. For 30 projections, the mean RC was 0.81($\pm$0.01[1]) and 0.77($\pm$0.01[1]) reconstructed with RDP and OSEM, respectively. For 60 projections, the mean RC was 0.80($\pm$0.00[1]) and 0.76($\pm$0.00[1]) reconstructed with RDP and OSEM, respectively. There was a statistically significant difference between the RCs obtained with the two reconstruction algorithms ($p<0.001$) as well as between the two projection sets using the students' t-test ($p<0.05$).

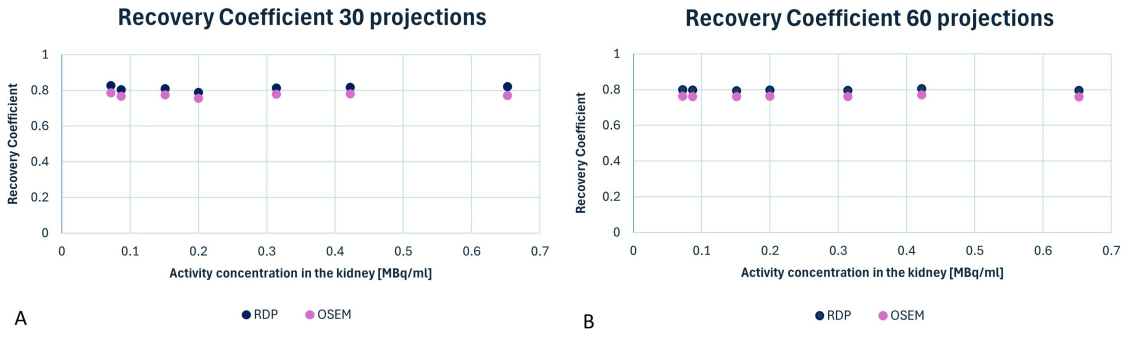

Figure 10: *RC for kidney 1 related to the activity concentrations. All images were reconstructed with RDP (blue dots) and OSEM (pink dots). Images collected with A: 30 projections, B: 60 projections.*

The RC did not vary with kidney and background activity concentration ratio, as seen in Figure 11. For 30 projections, the mean RC was 0.81($\pm$0.03[1]) and 0.78($\pm$0.03[1]) reconstructed with RDP and OSEM, respectively. For 60 projections, the mean RC was 0.80($\pm$0.03[1]) and 0.76($\pm$0.03[1]) reconstructed with RDP and OSEM, respectively. All kidney values can be seen in Appendix Table 8-13.

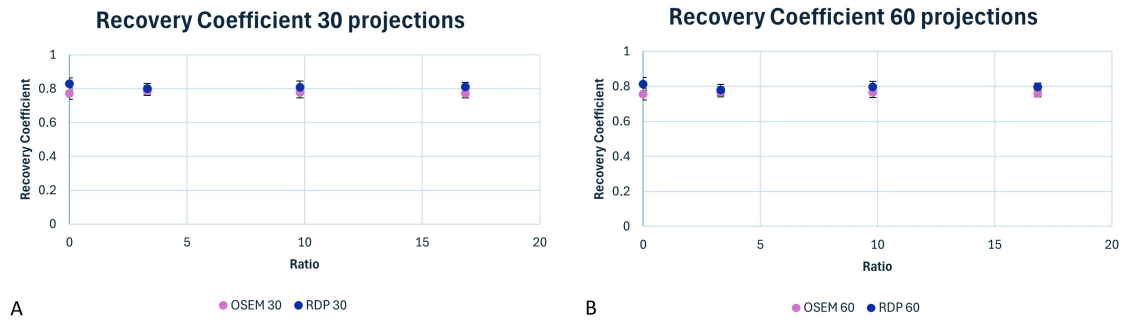

Figure 11: *The mean RC for kidneys 1-5 related to the activity concentrations ratio between the activity concentration in the kidneys and the background. The error bars indicate the range between the kidneys 1-5. All images were reconstructed with RDP (blue dots) and OSEM (pink dots). The first measurement was performed without background activity. Images collected with A: 30 projections, B: 60 projections.*

[1]Standard deviation

3.1 Recovery coefficient using small VOI method

The RC was higher using the small VOI method. For 30 projections, the mean RC was $0.81(\pm 0.01^{1})$ and $0.95(\pm 0.04^{1})$ for whole-segmented kidney and small VOIs, respectively. For 60 projections, the mean RC was $0.80(\pm 0.00^{1})$ and $0.92(\pm 0.02^{1})$ for whole-segmented kidney and small VOIs, respectively.

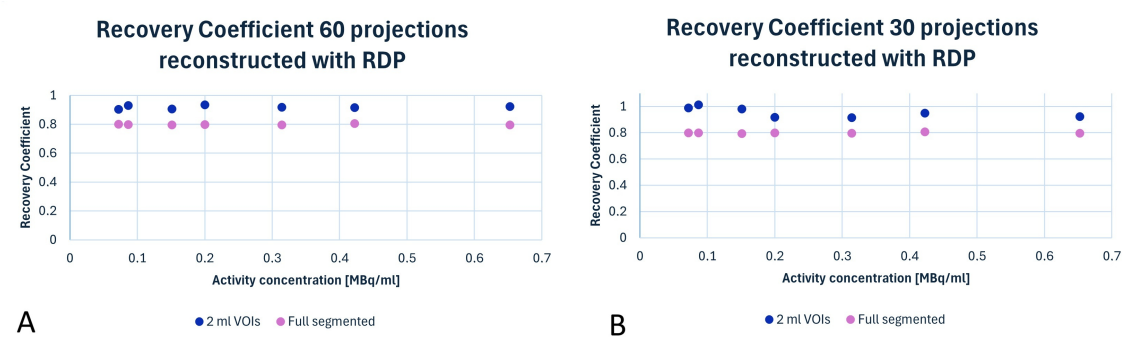

Figure 12: *The RC for kidney 1 related to the activity concentrations for both small VOIs (blue dots) and whole segmented kidney (pink dots). Images collected with A: 30 projections, B: 60 projections*

[1]Standard deviation

4 Discussion

The RC did not change with the activity concentration in the kidneys. This means that using different RCs at different imaging time points is unnecessary. The RC did not change between different ratios of the activity concentrations in the kidney and background. There was a statistically significant difference in the RC between 30 and 60 projections, where the 30 projections had slightly higher RC than the 60 projections. This might be due to more image noise in images collected with 30 projections. The number of subsets was reduced at 30 projections to get more projections per subset and improve convergence. Since the product of subsets and iterations is desired to be as close to 80 as possible, the number of iterations needed to be increased, which results in increased noise. Since the same VOI has been used for 30 and 60 projections, the difference is not due to manual segmentation.

According to EANM dosimetry guidelines, 60-120 projections should be used. Only determination of the RC is included in the present study and not the whole dosimetry workflow [32]. Wikberg et al found that there was a statistically significant difference in absorbed dose to the kidneys when using 30 projections compared to 120 projections though they questioned if the difference was clinically relevant. However, no difference was seen in the RC when simulated with 30 projections and 120 projections. [48]. The advantage of 30 projections is that the image collection is faster, while the advantage of 60 projections is that it provides better count statistics, if using the same frame duration. There was also a statistically significant difference between the reconstruction methods OSEM and RDP, where RDP yielded a higher RC value, mainly due to the fact that RDP has smoothing and edge-preserving effects. The RC must therefore be determined for different numbers of projections and depending on which reconstruction method is used.

One observer did all the segmentations, although the segmented volume changed between measurements. The percentage deviation in segmentation is shown in the Appendix in Table 5. This affects the uncertainty in the derived RC. Since the phantom was not shifted between 30 and 60 projections, the segmentation remained consistent between reconstruction techniques and projections, allowing the same VOI for the same activity concentration. There is also an uncertainty in the scale ($\pm$0.01 g), and the dose calibrator ($\pm$0.01 Bq). Despite this, the standard deviation for the RC was low, showing that the observer was consistent.

No statistically significant difference in the RC was shown between the kidney and background activity concentrations over the investigated ratio range. This indicates that the RC is stable regardless of background activity (i.e., kidney spill-in activity). This applies to backgrounds that do not have significant tumor uptake. High uptake by surrounding tumors, such as in the liver, may affect RC in the kidney. More studies that simulate high tumor burden, near the kidney, should therefore be done in the future.

That the RC varies with size and shape has been demonstrated in previous studies, as in the study by Gunes Y. et al., where an increased sphere diameter showed an increased RC [39]. During the 3D printing, kidneys 2, 4, and 5 were given the same shape, while kidney 3 was given another shape. Kidney 3 always had a higher RC in all measurements (as seen in the Appendix in Figure 13), probably due to the shape varying from the remaining kidneys, thus, the impact of PVE. The higher RC may also be due to the segmentation. The standard deviation for the RC for each kidney can be seen in Appendix Table 7. It would be good to investigate the RC with more varying shapes and sizes of kidney phantoms in future studies. With ethical permission, patient-specific RCs can be investigated where patients' kidneys are segmented, and the RC is simulated.

This study was based on the fillable volume when calculating the ratio between the kidney and the background, as the volume of the medulla and the total volume before the measurements could not be obtained. The ratio, therefore, needed to be calculated retrospectively for each kidney once the total volume had been determined, which meant that the ratios differed slightly from kidney to kidney. Furthermore, the ratios were not the same as planned. Despite this, the RC was shown not to be affected by different ratios. In the future, the total volume should be determined from the beginning so that each kidney can have the same ratio for a better comparison, even though this study showed that the RC is constant and unaffected by the ratio between the kidney and the background.

The 3D printing material for kidney 1 was slightly different from the remaining kidneys. It would be better to have all kidneys printed using the same material. Kidneys 2-5 were also printed afterward without the medulla to determine the total volume. When the kidney is printed, it can vary slightly depending on, among other things, the angle at which it was printed, thus affecting its weight. This means that the total volume of the kidney, including the medulla, is uncertain. These "empty" kidneys were only used for volume determination and were not filled and imaged with [^{177}Lu]-DOTATATE.

The small VOIs segmentation method showed a higher RC but also a higher standard deviation than the whole kidney segmentation, Appendix Table 6. In the case of a whole segmented kidney, the spill-out effect is more significant when segmenting at the edges of the kidney. In the case of the small VOI method, the VOIs are avoided near the edge, which minimizes the spill-out effect. However, AI-segmentation of the kidneys in voxel dosimetry is more time efficient than using the small-VOI method.

The clinical imaging protocol at Sahlgrenska University Hospital uses 60 projections and a frame duration of 40 seconds with Hermes RDP reconstruction. The RC for the kidneys using this protocol was determined to be 0.80.

5 Conclusion

The method for determination of the RC is considered reasonable. Sahlgrenska University Hospital's clinical imaging protocol uses Hermes RDP reconstruction with 60 projections and a 40-second frame time. Using this procedure, the RC was found to be 0.80. This study demonstrates that the kidney RC remains stable at the investigated activity concentrations and is consistent for the ratios between kidney and background used in this study. This means that the RC does not need to be adjusted between imaging time points. Furthermore, RDP reconstruction resulted in a higher RC than the OSEM reconstruction.

References

[1] Michael J et al. "Principles of diagnosis and management of neuroendocrine tumours". In: *Canadian medical association journal* 189.10 (2017). DOI: https://doi.org/10.1503/cmaj.160771.

[2] National Cancer Institute. *Neuroendocrine tumor*. URL: https://www.cancer.gov/pediatric-adult-rare-tumor/rare-tumors/rare-endocrine-tumor/carcinoid-tumor. (accessed: 24.01.2025).

[3] Peiwen Wu et al. "Epidemiologic trends of and factors associated with overall survival in patients with neuroendocrine tumors over the last two decades in the USA". In: *Endocrine connections research* 12.12 (2023). DOI: https://doi.org/10.1530/EC-23-0331.

[4] Arvind Dasari et al. "Trends in the incidence, prevalence, and survival outcomes in patients with neuroendocrine tumors in the United States". In: *Jama oncology* 3.10 (2017). DOI: 0.1001/jamaoncol.2017.0589.

[5] Sejin Ha et al. "Prediction of [177Lu]Lu-DOTA-TATE therapy response using the absorbed dose estimated from [177Lu]Lu-DOTA-TATE SPECT/CT in patients with metastatic neuroendocrine tumour". In: *European journal of nuclear medicine and molecular imaging physics* 11.14 (2024). DOI: https://doi.org/10.1186/s40658-024-00620-8.

[6] Satya Dasa et al. "177Lu-DOTATATE for the treatment of gastroenteropancreatic neuroendocrine tumors". In: *Expert review of gastroenterology and hepatology* 13.11 (2019). DOI: https://doi.org/10.1080/17474124.2019.1685381.

[7] Ravi K. Paluri and Robert B. Killeen. *Neuroendocrine tumor Lu-177-Dotatate therapy*. StatPearls Publishing, 2024. ISBN: NBK587368.

[8] Cleveland Clinic. *Peptide receptor radionuclide therapy (PRRT)*. URL: https://my.clevelandclinic.org/health/treatments/24073-peptide-receptor-radionuclide-therapy-prrt. (accessed: 27.01.2025).

[9] Wikipedia. *Peptide receptor radionuclide therapy*. URL: https://en.wikipedia.org/wiki/Peptide_receptor_radionuclide_therapy. (accessed: 24.01.2025).

[10] Milad Peer-Firozjaei et al. "Evaluation of dosimetric parameters for tumor therapy with 177Lu and 90Y radionuclides in gate Monte Carlo code". In: *Journal of biomedical physics and engineering* 11.3 (2021). DOI: https://doi.org/10.31661/jbpe.v0i0.2101-1256.

[11] Keunyoung Kim and Seong-Jang Kim. "Lu-177-based peptide receptor radionuclide therapy for advanced neuroendocrine tumors". In: *Nuclear medicine and molecular imaging* 52.3 (2018). DOI: https://doi.org/10.1007/s13139-017-0505-6.

[12] A. Tuba Kendi et al. "Therapy with 177Lu-DOTATATE: clinical implementation and impact on care of patients with neuroendocrine tumors". In: *American journal of roentgenology* 213.2 (2019). DOI: https://doi.org/10.2214/AJR.19.21123.

[13] Jean-Mathieu Beauregard. "Use of imaging-based dosimetry for personalising radiopharmaceutical therapy of cancer". In: *Cancer imaging* 22.67 (2022). DOI: https://doi.org/10.1186/s40644-022-00505-y.

[14] Anna Sundlöv et al. "Phase II trial demonstrates the efficacy and safety of individualized, dosimetry-based 177Lu-DOTATATE treatment of NET patients". In: *European journal of nuclear medicine and molecular imaging* 49.11 (2022). DOI: https://doi.org/10.1007/s00259-022-05786-w.

[15] MD Jana Vasković. *Kidneys*. URL: https://www.kenhub.com/en/library/anatomy/kidneys. (accessed: 03.02.2025).

[16] Wikipedia. *Kidney*. URL: https://en.wikipedia.org/wiki/Kidney. (accessed: 03.02.2025).

[17] Ken Hub. *Renal medulla*. URL: https://www.kenhub.com/en/library/anatomy/renal-medulla. (accessed: 22.04.2025).

[18] Cleveland Clinic. *Kidney*. URL: https://my.clevelandclinic.org/health/body/21824-kidney. (accessed: 03.02.2025).

[19] Britannica. *Nephron*. URL: https://www.britannica.com/science/nephron. (accessed: 03.02.2025).

[20] Ken Hub. *Renal cortex*. URL: https://www.kenhub.com/en/library/anatomy/renal-cortex. (accessed: 22.04.2025).

[21] Ken Hub. *Glomerulus*. URL: https://www.kenhub.com/en/library/anatomy/glomerulus. (accessed: 22.04.2025).

[22] Ken Hub. *Proximal convoluted tubule*. URL: https://www.kenhub.com/en/library/anatomy/proximal-convoluted-tubule. (accessed: 22.04.2025).

[23] Ken Hub. *Distal convoluted tubule*. URL: https://www.kenhub.com/en/library/anatomy/distal-convoluted-tubule. (accessed: 22.04.2025).

[24] National Cancer Institute. *Collecting duct*. URL: https://www.cancer.gov/publications/dictionaries/cancer-terms/def/collecting-duct. (accessed: 13.06.2025).

[25] Cleveland Clinic. *Erythropoietin*. URL: https://my.clevelandclinic.org/health/articles/14573-erythropoietin. (accessed: 03.02.2025).

[26] Cleveland Clinic. *Renin*. URL: https://my.clevelandclinic.org/health/body/22506-renin. (accessed: 03.02.2025).

[27] PioM. *Kidney*. Wikimedia commons. Licensed under CC BY-SA 3.0. 2007. URL: https://commons.wikimedia.org/wiki/File:Kidney_PioM.png.

[28] Smart Servier Medical Art. *Urinary system – nephron 2*. Wikimedia commons. Licensed under CC BY 3.0. URL: https://commons.wikimedia.org/wiki/File:Urinary_system_-_Nephron_2_--_Smart-Servier.png.

[29] Peter Frøhlich Staanum et al. "Practical kidney dosimetry in peptide receptor radionuclide therapy using [177Lu] Lu-DOTATOC and [177Lu]Lu-DOTATATE with focus on uncertainty estimates". In: *European journal of nuclear medicine and molecular imaging physics* 8.78 (2021). DOI: https://doi.org/10.1186/s40658-021-00422-2.

[30] Katarina Sjögreen Gleisner et al. “EANM dosimetry committee recommendations for dosimetry of 177Lu-labelled somatostatin-receptor- and PSMA-targeting ligands”. In: *European journal of nuclear medicine and molecular imaging* 49.6 (2022). DOI: https://doi.org/10.1007/s00259-022-05727-7.

[31] Wikipedia. *Single-photon emission computed tomography*. URL: https://en.wikipedia.org/wiki/Single-photon_emission_computed_tomography. (accessed: 12.05.2025).

[32] M. Bardies and J.I. Gear z. “Scientific developments in imaging and dosimetry for molecular radiotherapy”. In: *Clinical oncology* 33.2 (2021). DOI: 10.1016/j.clon.2020.11.005.

[33] Keamogetswe Ramonaheng, Johannes A. van Staden, and Hanlie du Raan. “The effect of calibration factors and recovery coefficients on 177Lu SPECT activity quantification accuracy: a Monte Carlo study”. In: *European journal of nuclear medicine and molecular imaging physics* 8.27 (2021). DOI: https://doi.org/10.1186/s40658-021-00365-8.

[34] Erick Mora-Ramirez et al. “Comparison of commercial dosimetric software platforms in patients treated with 177Lu-DOTATATE for peptide receptor radionuclide therapy”. In: *Medical physics* 47.9 (2020). DOI: http://dx.doi.org/10.1002/mp.14375.

[35] Selma Curkic Kapidzic et al. “Kidney dosimetry in [177Lu]Lu-DOTA-TATE therapy based on multiple small VOIs”. In: *Physica medica* 120 (2024). DOI: 10.1016/j.ejmp.2024.103335.

[36] Wikipedia. *Time-activity curve*. URL: https://en.wikipedia.org/wiki/Time-activity_curve. (accessed: 28.03.2025).

[37] E J Hoffman and M E Phelps S C Huang. “Quantitation in positron emission computed tomography: 1. effect of object size”. In: *Journal of computer assisted tomography* 3.3 (1979). DOI: 10.1097/00004728-197906000-00001.

[38] Marine Soret, Stephen L. Bacharach, and Irene Buvat. “Partial-volume effect in PET tumor imaging*”. In: *Journal of nuclear medicine* 48.6 (2007). DOI: https://doi.org/10.2967/jnumed.106.035774.

[39] Gunes Yavuz et al. “Calculation of recovery coefcients for partial volume effect correction in PET/CT imaging using a customized anthropomorphic body phantom”. In: *Biomedical engineering onLine* 24.20 (2025). DOI: https://doi.org/10.1186/s12938-025-01330-7.

[40] Alexandre R. Krempser et al. “Recovery coefficients determination for partial volume effect correction in oncological PET/CT images considering the effect of activity outside the field of view”. In: *Annals of nuclear medicine* 27 (2013). DOI: https://doi.org/10.1007/s12149-013-0773-x.

[41] Johannes Tran-Gia, Susanne Schlögl, and Michael Lassmann. “Design and fabrication of kidney phantoms for internal radiation dosimetry using 3D printing technology”. In: *European journal of nuclear medicine and molecular imaging physics* 57.12 (2016). DOI: https://doi.org/10.2967/jnumed.116.178046.

[42] Lovisa Jessen et al. “3D printed non-uniform anthropomorphic phantoms for quantitative SPECT”. In: *European journal of nuclear medicine and molecular imaging physics* 11.8 (2024). DOI: https://doi.org/10.1186/s40658-024-00613-7.

[43] Hermes Medical Solution. *Voxel dosimetry - personalized dosimetry in minutes*. URL: https://www.hermesmedical.com/our-software/dosimetry/voxel-dosimetry/. (accessed: 20.05.2025).

[44] Hermes Medical Solutions. *Our software*. URL: https://www.hermesmedical.com/our-software/. (accessed: 12.03.2025).

[45] Hermes Medical Solution. *Hermia SPECT reconstruction*. URL: https://www.hermesmedical.com/media/white-papers/spect-reconstruction/. (accessed: 30.04.2025).

[46] Hermes Medical Solutions. *User handbook hybrid recon 5.0*. 2023.

[47] Lovisa Jessen et al. “A validation protocol for 177Lu-SPECT image quantification as a basis for multi-centre kidney dosimetry”. In: *Physics in medicine and biology* 70.11 (2025). DOI: 10.1088/1361-6560/add708.

[48] Emma Wikberg et al. “Improvements of 177Lu SPECT images from sparsely acquired projections by reconstruction with deep-learninggenerated synthetic projections”. In: *European journal of nuclear medicine and molecular imaging* 11.53 (2024). DOI: https://doi.org/10.1186/s40658-024-00655-x.

Appendix

Table 4: SPECT imaging setup

Energy	[^{177}Lu][113 and 208].EM	
Patient location	Feet First Supine	
Mode	H	
Body Contour	✓	
Scan on extender only		
Body part	ABDOMEN	
Startat	0 deg	
Acquire CT	✓	
Emission First	✓	
CT range	Full	
Select on	✓	
Scout		
Zoom	1	
Matrix	128x128	
Pan Y	0	
Continous/Dynamic		
Number o FOVs	1	
Rough Overlap	4	
Direction	Table Out	
FOV time multiplier	1	
Height	Absolute 94,0 cm	
Total angular range	360	
View angle	12	
Number of views	30	or 60
Direction	CW	
Detector Settings	Detector 1 och Detector 2	

Table 5: Percentage deviation in segmentation volume based on the total volume of the kidney. This shows how much the drawn volume deviated from the true volume. For kidney 1, there are eight segmentations from which the data is based, while for kidneys 2-5, there are four segmentations for each kidney from which the data is based.

	Kidney 1 [%]	Kidney 2 [%]	Kidney 3 [%]	Kidney 4 [%]	Kidney 5 [%]
Range	4.72-9.43	0.29-4.65	0.79-5.34	1.27-7.60	0.34-2.98
Mean	7.19	1.68	2.48	3.81	1.48

Table 6: The coefficient of variation for the kidneys using either whole kidney segmentation method or small VOI method using 2 mL VOIs.

Whole Kidney Segmentation			
OSEM 30 [%]	OSEM 60 [%]	RDP 30 [%]	RDP 60[%]
1.30	0.44	1.52	1.17
2 mL VOIs segmentation			
OSEM 30 [%]	OSEM 60 [%]	RDP 30 [%]	RDP 60[%]
3.62	1.08	3.82	1.52

Table 7: The standard deviation of RC for the four different measurements for kidneys 2-5.

OSEM				
	Kidney 2	Kidney 3	Kidney 4	Kidney 5
30 Projections	0.01	0.01	0.01	0.01
60 Projections	0.01	0.01	0.01	0.01
RDP				
	Kidney 2 [%]	Kidney 3 [%]	Kidney 4 [%]	Kidney 5 [%]
30 Projections	0.02	0.02	0.01	0.01
60 Projections	0.02	0.02	0.01	0.01

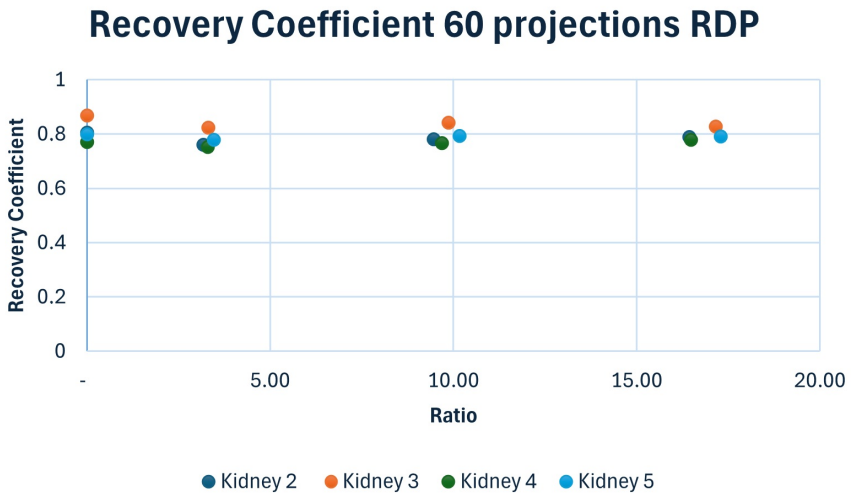

Figure 13: *The RC for kidneys 2-5 related to the activity concentrations ratio between the activity concentration in the kidneys and the background. All images were reconstructed with RDP and 60 projections.*

Table 8: Measurement results for kidney 1 at 30 projections with OSEM and RDP. AC (true) is the activity concentration in the total volume of the kidney that was measured at the time of injection. It is then decay corrected for each day. The same applies to the background. VOI is the size of the segmentation and AC (measured) is the activity concentration obtained through the segmentation.

Day	Reconstruction	AC (true) [MBq/mL]	AC (Measured) [MBq/mL]	Background AC [MBq/mL]	VOI [mL]	Recovery
D0	OSEM	0.77	0.59	0	113	0.76
D2	OSEM	0.65	0.50	0.048	112	0.77
D6	OSEM	0.42	0.33	0.032	111	0.78
D9	OSEM	0.31	0.24	0.023	113	0.78
D13	OSEM	0.20	0.15	0.015	116	0.75
D16	OSEM	0.15	0.12	0.011	114	0.77
D21	OSEM	0.087	0.067	0.0064	114	0.77
D23	OSEM	0.072	0.057	0.0053	116	0.76
D0	RDP	0.77	0.63	0	113	0.82
D2	RDP	0.65	0.54	0.048	112	0.82
D6	RDP	0.42	0.35	0.032	111	0.82
D9	RDP	0.31	0.26	0.023	113	0.81
D13	RDP	0.20	0.16	0.015	116	0.79
D16	RDP	0.15	0.12	0.011	114	0.81
D21	RDP	0.087	0.070	0.0064	114	0.80
D23	RDP	0.072	0.059	0.0053	116	0.83

Table 9: Measurement results for kidney 1 at 60 projections with OSEM and RDP. AC (true) is the activity concentration in the total volume of the kidney that was measured at the time of injection. It is then decay corrected for each day. The same applies to the background. VOI is the size of the segmentation and AC (measured) is the activity concentration obtained through the segmentation.

Day	Reconstruction	AC (true) [MBq/mL]	AC (Measured) [MBq/mL]	Background AC [MBq/mL]	VOI [mL]	Recovery
D0	OSEM	0.77	0.59	0	113	0.76
D2	OSEM	0.65	0.50	0.048	112	0.76
D6	OSEM	0.42	0.33	0.032	111	0.77
D9	OSEM	0.31	0.24	0.023	113	0.76
D13	OSEM	0.20	0.15	0.015	116	0.76
D16	OSEM	0.15	0.12	0.011	114	0.76
D21	OSEM	0.087	0.066	0.0064	114	0.76
D23	OSEM	0.072	0.055	0.0053	116	0.79
D0	RDP	0.77	0.63	0	113	0.82
D2	RDP	0.65	0.52	0.048	112	0.80
D6	RDP	0.42	0.34	0.032	111	0.81
D9	RDP	0.31	0.25	0.023	113	0.80
D13	RDP	0.20	0.16	0.015	116	0.80
D16	RDP	0.15	0.12	0.011	114	0.79
D21	RDP	0.087	0.069	0.0064	114	0.80
D23	RDP	0.072	0.058	0.0053	116	0.80

Table 10: Measurement results for kidney 2 (K2) at 30 and 60 projections with OSEM and RDP. AC (true) is the activity concentration in the total volume of the kidney that was measured at the time of injection. It is then decay corrected for each day. The same applies to the background. VOI is the size of the segmentation and AC (measured) is the activity concentration obtained through the segmentation.

Ratio	Reconstruction	BG [MBq/mL]	AC K2 (true) [MBq/mL]	AC K2 (measured) [MBq/mL]	VOI K2 [mL]	K2 Recovery
0	OSEM 30	0	0.64	0.49	120	0.76
16.44	OSEM 30	0.035	0.58	0.44	117	0.77
9.46	OSEM 30	0.055	0.52	0.40	115	0.77
3.17	OSEM 30	0.15	0.47	0.37	116	0.78
0	RDP 30	0	0.64	0.53	120	0.82
16.44	RDP 30	0.035	0.58	0.47	117	0.81
9.46	RDP 30	0.055	0.52	0.42	115	0.80
3.17	RDP 30	0.15	0.47	0.37	116	0.79
Ratio	**Reconstruction**	**BG [MBq/mL]**	**AC K2 (true) [MBq/mL]**	**AC K2 (measured) [MBq/mL]**	**VOI K2 [mL]**	**K2 Recovery**
0	OSEM 60	0	0.65	0.49	120	0.75
16.44	OSEM 60	0.035	0.58	0.44	117	0.75
9.46	OSEM 60	0.055	0.52	0.39	115	0.75
3.17	OSEM 60	0.15	0.47	0.35	116	0.75
0	RDP 60	0	0.65	0.53	120	0.80
16.44	RDP 60	0.035	0.58	0.46	117	0.79
9.46	RDP 60	0.055	0.52	0.41	115	0.78
3.17	RDP 60	0.15	0.47	0.36	116	0.76

Table 11: Measurement results for kidney 3 (K3) at 30 and 60 projections with OSEM and RDP. AC (true) is the activity concentration in the total volume of the kidney that was measured at the time of injection. It is then decay corrected for each day. The same applies to the background. VOI is the size of the segmentation and AC (measured) is the activity concentration obtained through the segmentation.

Ratio	Reconstruction	BG [MBq/mL]	AC K3 (true) [MBq/mL]	AC K3 (measured) [MBq/mL]	VOI K3 [mL]	K3 Recovery
0	OSEM 30	0	0.67	0.55	109	0.83
17.15	OSEM 30	0.035	0.60	0.49	111	0.81
9.87	OSEM 30	0.055	0.55	0.45	107	0.83
3.31	OSEM 30	0.15	0.49	0.41	104	0.83
0	RDP 30	0	0.67	0.59	109	0.89
17.15	RDP 30	0.035	0.60	0.51	111	0.85
9.87	RDP 30	0.055	0.54	0.47	107	0.86
3.31	RDP 30	0.15	0.49	0.42	104	0.85
Ratio	**Reconstruction**	**BG [MBq/mL]**	**AC K3 (true) [MBq/mL]**	**AC K3 (measured) [MBq/mL]**	**VOI K3 [mL]**	**K3 Recovery**
0	OSEM 60	0	0.68	0.55	109	0.81
17.15	OSEM 60	0.035	0.60	0.48	111	0.79
9.87	OSEM 60	0.055	0.54	0.44	107	0.81
3.31	OSEM 60	0.15	0.49	0.40	104	0.81
0	RDP 60	0	0.68	0.59	109	0.87
17.15	RDP 60	0.035	0.60	0.50	111	0.83
9.87	RDP 60	0.055	0.55	0.46	107	0.84
3.31	RDP 60	0.15	0.49	0.40	104	0.82

Table 12: Measurement results for kidney 4 (K4) at 30 and 60 projections with OSEM and RDP. AC (true) is the activity concentration in the total volume of the kidney that was measured at the time of injection. It is then decay corrected for each day. The same applies to the background. VOI is the size of the segmentation and AC (measured) is the activity concentration obtained through the segmentation.

Ratio	Reconstruction	BG [MBq/mL]	AC K4 (true) [MBq/mL]	AC K4 (measured) [MBq/mL]	VOI K4 [mL]	K4 Recovery
0	OSEM 30	0	0.33	0.24	119	0.74
16.48	OSEM 30	0.018	0.30	0.22	114	0.74
9.69	OSEM 30	0.028	0.27	0.20	115	0.75
3.29	OSEM 30	0.074	0.24	0.19	114	0.76
0	RDP 30	0	0.33	0.49	119	0.79
16.48	RDP 30	0.018	0.30	0.44	114	0.78
9.69	RDP 30	0.028	0.27	0.40	115	0.77
3.29	RDP 30	0.074	0.24	0.36	114	0.75
Ratio	**Reconstruction**	**BG [MBq/mL]**	**AC K4 (true) [MBq/mL]**	**AC K4 (measured) [MBq/mL]**	**VOI K4 [mL]**	**K4 Recovery**
0	OSEM 60	0	0.33	0.24	119	0.72
16.48	OSEM 60	0.018	0.30	0.22	114	0.74
9.69	OSEM 60	0.028	0.27	0.20	115	0.74
3.29	OSEM 60	0.074	0.24	0.18	114	0.74
0	RDP 60	0	0.33	0.49	119	0.77
16.48	RDP 60	0.018	0.30	0.44	114	0.78
9.69	RDP 60	0.028	0.27	0.40	115	0.78
3.29	RDP 60	0.074	0.24	0.36	114	0.77

Table 13: Measurement results for kidney 5 (K5) at 30 and 60 projections with OSEM and RDP. AC (true) is the activity concentration in the total volume of the kidney that was measured at the time of injection. It is then decay corrected for each day. The same applies to the background. VOI is the size of the segmentation and AC (measured) is the activity concentration obtained through the segmentation.

Ratio	Reconstruction	BG [MBq/mL]	AC K5 (true) [MBq/mL]	AC K5 (measured) [MBq/mL]	VOI K5 [mL]	K5 Recovery
0	OSEM 30	0	0.35	0.26	117	0.76
17.29	OSEM 30	0.018	0.31	0.24	114	0.77
10.17	OSEM 30	0.028	0.28	0.22	112	0.77
3.46	OSEM 30	0.074	0.26	0.20	111	0.79
0	RDP 30	0	0.35	0.28	117	0.81
17.29	RDP 30	0.018	0.31	0.25	114	0.81
10.17	RDP 30	0.028	0.28	0.23	112	0.80
3.46	RDP 30	0.074	0.26	0.20	111	0.80
Ratio	**Reconstruction**	**BG [MBq/mL]**	**AC K5 (true) [MBq/mL]**	**AC K5 (measured) [MBq/mL]**	**VOI K5 [mL]**	**K5 Recovery**
0	OSEM 60	0	0.35	0.26	117	0.74
17.29	OSEM 60	0.018	0.31	0.24	114	0.76
10.17	OSEM 60	0.028	0.28	0.22	112	0.77
3.46	OSEM 60	0.074	0.26	0.20	111	0.77
0	RDP 60	0	0.35	0.28	117	0.80
17.29	RDP 60	0.018	0.31	0.25	114	0.79
10.17	RDP 60	0.028	0.28	0.22	112	0.79
3.46	RDP 60	0.074	0.26	0.20	111	0.78